

¹³B. R. Judd, *Operator Techniques in Atomic Spectroscopy* (McGraw-Hill, New York, 1963), pp. 206–209.

¹⁴A linear function was chosen here because the known E^1 values for the $M(\text{III})$ complexes are to a good approximation a linearly increasing function of q for each series.

¹⁵B. G. Wybourne, *Spectroscopic Properties of Rare Earths* (Wiley, New York, 1965), pp. 41 and 49–62.

¹⁶More recent as yet unpublished information on the experimental values for E^1 for certain complexes of the higher An (III) ions causes us to lower our estimate here from $6.6 \times 10^3 \text{ cm}^{-1}$ as given in Ref. 9 to this $5.0 \times 10^3 \text{ cm}^{-1}$ value.

¹⁷See, B. Fricke and J. T. Waber [Actinide Rev. 1, 433 (1971)] for the latest and most thorough review of this subject.

¹⁸G. T. Seaborg, J. L. Crandall, P. R. Fields, A. Ghiorso, O. L. Keller, and R. A. Penneman, Proceedings

of the Atoms for Peace Conference, Geneva, 1971 (unpublished).

¹⁹In this direct linearization of the $\Delta_{M^1}E(q)$ data points, $\Delta_{M^1}E(0)$ for La and $\Delta_{M^1}E(14)$ for Lu were omitted for reasons discussed later in the development of the text.

²⁰The $\Delta_{M^1}E(q)$ data point for Th was omitted in this determination of line b for reasons discussed later in the development of the text.

²¹N. Spector, J. Opt. Soc. Am. 56, 341 (1966).

²²B. W. Bryant, J. Opt. Soc. Am. 55, 771 (1965).

²³N. Spector, J. Opt. Soc. Am. 57, 312 (1965).

²⁴B. R. Judd, Phys. Rev. 125, 613 (1962).

²⁵M. Mayer, Phys. Rev. 60, 184 (1941).

²⁶L. J. Nugent, P. G. Laubereau, G. K. Werner, and K. L. Vander Sluis, J. Organometal. Chem. (Amsterdam) 27, 365 (1971).

PHYSICAL REVIEW A

VOLUME 6, NUMBER 1

JULY 1972

Ultrasoft-X-Ray Reflection, Refraction, and Production of Photoelectrons (100–1000-eV Region)*

Burton L. Henke

University of Hawaii, Honolulu, Hawaii 96822

(Received 14 February 1972)

The reflection, refraction, and associated production of photoelectrons by ultrasoft x rays (10–100 Å) can be important bases for the determination of material constants such as the linear x-ray absorption coefficients and the electron mean free paths. These may then be used to establish directly the photoionization cross sections and the electron-collision cross sections which account for the dominant energy-absorbing processes within solids for this energy region. Because the effective sample depths for these interactions are typically less than 100 Å, they constitute an important practical basis for surface characterization. By applying the exact theory for the reflection-refraction of a plane electromagnetic wave at an absorbing dielectric interface to the shorter-wavelength region (<10 Å), it can be shown that the conventional approximate theory of x-ray reflection is adequate. However, the more exact theory must be applied in the region of longer x-ray wavelengths (>50 Å). Although the derivations of the exact theory are tedious, the results can be expressed in relatively simple form as functions of two material constants α and γ , which are identifiable as the unit decrements to a complex dielectric constant, of the grazing-incidence angle, and of a parameter which is a function of this grazing angle and which becomes the angle of refraction for small angles of incidence. X-ray absorption coefficients and electron mean-free-path values have been determined from x-ray reflection and refraction and photoelectron excitation data. These values have been shown to agree reasonably well with such material constants as determined by transmission measurements through thin samples.

I. INTRODUCTION

It is well known that x rays do reflect from surfaces with high efficiency in the grazing-incidence region. The characteristic reflectance curve, which falls off to zero value with increasing angle, is the basis for an important method for determining the optical constants of the reflecting medium and its surface structure.^{1,2} Also, a precise knowledge of this "total-reflection" characteristic curve is important in the design of mirror monochromators,³ of optimized diffraction gratings, and of astronomical telescope systems for the x-ray

region.

As will be described below, the refracted x-ray beam, when used to produce photoelectrons, can also be an important basis for the determination of certain constants of the medium and of its surface structure.⁴

In order to relate experimental reflection, refraction, and associated photoelectron excitation data to the optical constants, one may apply a relatively simple electromagnetic model based upon approximations permitted by the small values of the grazing-incidence angles and of complex refractive-index unit decrements which obtain for the

conventional x-ray region.⁵ Although this approach has been proven to be satisfactory for x-ray wavelengths below 10 Å, it may not be sufficiently accurate for the ultrasoft-x-ray region of 10–100 Å. Rather, one may need to apply the exact solutions of the electromagnetic theory to the x-ray interaction as a boundary-value problem.^{6,7}

In this paper, the results of both the approximate and exact electromagnetic theories will be compared for the ultrasoft-x-ray region and then applied to the determination of material constants from x-ray reflection and photoelectron-intensity measurements.

II. MODEL FOR PHOTOELECTRON-INTENSITY ANALYSIS

In Fig. 1 is shown the essential geometry of the model adopted here for the generation of the unscattered no-loss photoelectron signal (the spectrographic photoelectron intensity "peak"). Monoenergetic parallel x radiation of wavelength λ is incident upon a plane surface at an angle ϕ , refracting into a homogeneous isotropic sample with angle ϕ' . The linear x-ray absorption coefficient for this radiation within the sample is equal to μ . In a sample layer at depth z and thickness dz , photoelectrons are generated within an effective sample area which is the projection of the limiting slit area A_0 . The effective atomic cross section for the creation of q -type photoelectrons is τ_q . The number per unit volume of atoms within the sample which can emit q -type photoelectrons is ρ_q . [Note that if the angular distribution of the particular q -type photoelectron being measured is essentially isotropic, τ_q is equal to the partial photoionization cross section for either a single- or multiple-ionization

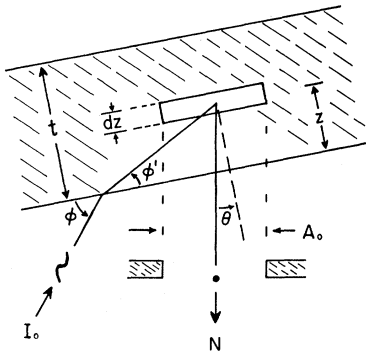


FIG. 1. Geometry for the production of photoelectrons. I_0 is the number of photons/cm² sec reaching the sample from a monochromatic x-ray source. N is the number of photoelectrons/sec which are accepted by the electron spectrograph in generating a no-loss photoelectron "peak." A_0 is a limiting slit at the sample which is an effective, projected area of the sample as presented to the entrance annular slit of the spectrograph.

process σ_q , e. g., σ_{1s} , σ_{2s} , $\sigma_{2p1/2}$, etc. For a non-isotropic distribution, τ_q is equal to the differential cross section multiplied by 4π , i. e., $4\pi(d\sigma_q/d\omega)_\psi$, where $d\omega$ is the differential solid angle and ψ is the angle between the incident photons and the emitted no-loss photoelectrons being measured.]

For the photoelectron energies of interest here, viz., in the 100–1000-eV region, elastic scattering and backreflection or refraction of the photoelectrons are considered to be of negligible effect on the no-loss peak signal; therefore, the fraction of the photoelectrons that originates at depth z and passes through the surface can be expressed as $e^{-\epsilon z}$. ϵ is a linear electron-attenuation coefficient, characteristic of the electron energy and of the sample, and is related to the mean free path and to the atomic ionization cross sections. Finally, the small solid angle around the emission angle θ , subtended at the sample by the effective entrance slit annulus of the spectrograph, is defined here as ω .

The contribution dN to the no-loss photoelectron signal may now be written as

$$dN = S(1-R)\rho_q\tau_q \frac{\sin\phi}{\sin\phi'\cos\theta} e^{-hz} dz, \quad (1)$$

where

$$S = I_0 A_0 (\omega/4\pi) \quad (\text{an instrument constant})$$

and

$$h = \mu/\sin\phi' + \epsilon/\cos\theta.$$

In Eq. (1), R is the Fresnel coefficient for x-ray reflection, i. e., the fraction of the I_0 intensity that does not enter the sample owing to reflection. R differs from zero value only in the small-angle region.

Integrating (1) over the sample thickness t yields

$$N_t = S(1-R) \left(\frac{\rho_q\tau_q}{\epsilon} \right) \frac{\sin\phi(1-e^{-ht})}{\sin\phi' + \mu(\cos\theta)/\epsilon}. \quad (2)$$

(Note that we will not consider here the special case of thin-film interference which may be significant, in the small- ϕ region, when sample thickness t is of the order of 100 Å.)

For the large-angle ϕ region, and for $\theta=0$ (the usual geometry in photoelectron spectroscopy), Eq. (2) becomes

$$N_t = S(\rho_q\tau_q/\epsilon)(1-e^{-\epsilon t}) \quad (3)$$

since, for large ϕ , $\sin\phi \approx \sin\phi' \gg \mu/\epsilon$. In this case, the x rays penetrate much further than the effective escape depths of the photoelectrons; consequently, x-ray absorption effects become negligible. For thick samples, the photoelectron signal may be expressed simply as

$$N = S(\rho_q\tau_q/\epsilon) = S\rho_q\tau_q\Lambda, \quad (4)$$

where the linear electron-attenuation coefficient ϵ may be defined by

$$\epsilon = \sum \rho_i Q_i = 1/\Lambda ; \quad (5)$$

ρ_i is the number of atoms of type i per unit volume, Q_i is their atomic ionization cross section, and Λ is the mean free path for the q -type photoelectrons being measured.

For small ϕ , ϕ' is not equal to ϕ and must be determined by an analysis of the refraction of a plane electromagnetic wave at the boundary of the sample.

To be exact, in Eq. (2), ϕ' defines the direction of energy flow within the medium (i. e., that of the Poynting's vector) and this direction is not necessarily perpendicular to the equiphase planes. R should be determined from the exact Fresnel equations, and, in a precise analysis, μ may not be taken as a constant but rather as a function of the incident angle ϕ .

Qualitatively, the equations for N above predict that the no-loss photoelectron peak intensity should be a constant as the sample is rotated in the large- ϕ region. In the small- ϕ region, however, a peak in photoelectron intensity is predicted as resulting from the fact that near the "total-reflection" region the x-ray beam is refracted at a small angle from the surface, thus creating more photoelectrons within the escape depth. These characteristics are demonstrated in the experimental measurement of photoelectron line intensity vs ϕ , presented in Fig. 2. The line at 1404 eV was excited by Al $K\alpha$ (1487-eV) photons from the Au $4f_{7/2}$ level (from a "thick" evaporated gold film).

Before attempting to interpret such data quantitatively, we will consider in a general way, and for the ultrasoft-x-ray region, the descriptions of x-ray reflection and refraction.

III. X-RAY REFLECTION-REFRACTION THEORY

There is good experimental evidence that one can satisfactorily treat the x-ray interaction described above as a boundary-value problem for the reflection and refraction of a plane electromagnetic wave at an absorbing medium.

For example, the author and others^{1,2} have obtained good fits to experimental x-ray reflection curves with theoretical ones based upon the Fresnel equations and refractive indices derived from the quantum-mechanical dispersion theory.

A. Approximate Solutions

In this section, a conventional approximate, but complete, treatment of the boundary-value problem for the refraction of x rays will be presented in order to illustrate the nature of the assumptions and approximations that are made. In Sec. III B, these will be shown to be valid for the shorter-wavelength region.

In this approach a complex index of refraction is used, given by

$$n = 1 - \delta - i\beta .$$

It is assumed that the unit decrements δ and β are very small as compared to unity. The unpolarized x-ray beam is assumed to reflect and to refract precisely as does a beam polarized with its electric vector normal to the plane of incidence so that only an analysis for this polarized component need be given.

The electric vector E_2 for the wave inside the boundary (medium 2) may be described as

$$E_2 = E_2(0) e^{i(\omega t - \vec{k}_2 \cdot \vec{r})} , \quad (6)$$

where

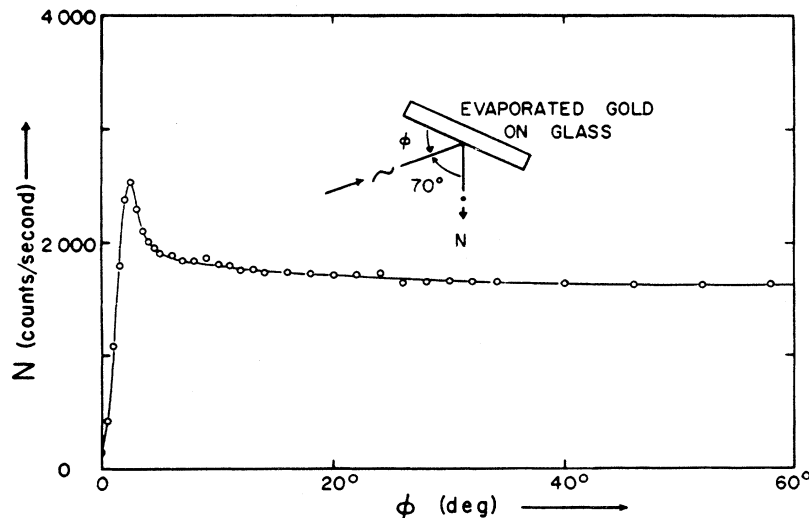


FIG. 2. Illustrating, for a homogeneous isotropic sample, the sharp increase in photoelectron intensity in the critical reflection "cutoff" region near ϕ_c , and the characteristically constant photoelectron signal in the large- ϕ region.

$$\vec{k}_2 \cdot \vec{r} = k_{2x}x + k_{2z}z.$$

Now we have

$$k_2^2 = k_{2x}^2 + k_{2z}^2 = n^2 k_1^2. \quad (7)$$

At the boundary, the tangential (x) components of the external and internal electric fields must be equal, including their phase. Therefore, we have

$$k_{2x} = k_{1x}. \quad (8)$$

From (7) and (8), we may write

$$k_2^2 = k_{1x}^2 + k_{2z}^2 = k_{1x}^2 [(1 - 2\delta - 2i\beta)/\cos^2\phi]. \quad (9)$$

And for ϕ small, (9) becomes

$$k_{1x}^2 + k_{2z}^2 = k_{1x}^2 (1 - 2\delta + \phi^2 - 2i\beta). \quad (10)$$

Since $k_{1x} \approx k_1$, (10) becomes

$$k_{2z} = k_1 (\phi^2 - 2\delta - 2i\beta)^{1/2} = k_1 (a_0 - ib_0). \quad (11)$$

Therefore, (6) may be written

$$E_2 = E_2(0) \exp\{i[\omega t - k_1(x + a_0 z)]\} \exp(-k_1 b_0 z), \quad (12)$$

and a_0 and b_0 can be evaluated as

$$a_0^2 = \frac{1}{2} \{[(\phi^2 - 2\delta)^2 + 4\beta^2]^{1/2} + (\phi^2 - 2\delta)\} \quad (13)$$

and

$$b_0^2 = \frac{1}{2} \{[(\phi^2 - 2\delta)^2 + 4\beta^2]^{1/2} - (\phi^2 - 2\delta)\} = (\beta/a_0)^2. \quad (14)$$

Finally, from (12), we note

$$\tan\phi' = a_0 \approx \phi'. \quad (15)$$

Multiplying (12) by its complex conjugate, we obtain

$$I_2 \sim E_2^2(0) e^{-2k_1 b_0 z}. \quad (16)$$

Since $\phi' = a_0$ and $k_1 = 2\pi/\lambda$, we have

$$2k_1 b_0 z = 2k_1 a_0 b_0 z / a_0 = (4\pi\beta/\lambda) r.$$

Defining $\mu = 4\pi\beta/\lambda$, we have

$$2k_1 b_0 z = \mu r.$$

Equation (16) becomes the usual absorption law

$$I_2 \sim E_2^2(0) e^{-\mu r}. \quad (17)$$

Returning to Eq. (2) for ϕ small and replacing $\sin\phi'$ by ϕ' ($= a_0$), we obtain for thick samples

$$N = S(1 - R_0) \left(\frac{\rho_q \tau_q}{\epsilon} \right) \frac{\phi}{a_0 + \mu(\cos\theta)/\epsilon}, \quad (18)$$

where, from the approximated Fresnel equations,⁵

$$R_0 = [a_0^2(\phi - a_0)^2 + \beta^2] / [a_0^2(\phi + a_0)^2 + \beta^2]. \quad (19)$$

Combining (18) and (19),

$$\begin{aligned} N &= S \left(\frac{\rho_q \tau_q}{\epsilon} \right) \frac{4\phi^2 a_0^3}{[a_0^2(\phi + a_0)^2 + \beta^2][a_0 + \mu(\cos\theta)/\epsilon]} \\ &= S \left(\frac{\rho_q \tau_q}{\epsilon} \right) F(\phi), \end{aligned} \quad (20)$$

where $F(\phi) \rightarrow 1$ for $\phi \gg (2\delta)^{1/2}$.

$F(\phi)$ may be expressed as a universal function:

$$F(x, y, z) = \frac{16x^2 A^3}{[4A^2(x+A)^2 + y^2] (A+z)}, \quad (21)$$

where

$$x = \phi / (2\delta)^{1/2}, \quad (22)$$

$$y = \beta / \delta, \quad (23)$$

$$z = \mu \cos\theta / \epsilon (2\delta)^{1/2} = 2\pi y (2\delta)^{1/2} (\Lambda/\lambda) \cos\theta, \quad (24)$$

$$A^2 = \frac{1}{2} \{[(x^2 - 1)^2 + y^2]^{1/2} + (x^2 - 1)\}. \quad (25)$$

The universal function $F(x, y, z)$ predicts the intensity of the no-loss photoelectron signal N as normalized to unity for its constant value in the large-angle region for which $\phi \gg (2\delta)^{1/2}$. $F(x, y, z)$ is plotted in Fig. 3 as a function of x for typical values of y and z . [The characteristic value $(2\delta)^{1/2}$ is often described as "a critical angle for total reflection" because it approximately defines the angular region for which the reflected intensity "cuts off."]

The results of this section, based upon conventional simplifying assumptions and approximations, have been found to be satisfactory for the shorter x-ray wavelengths. How to determine precisely the wavelength region for which these results are valid will be established in Sec. III B.

B. Exact Solutions

Many approaches and formalisms have been used in solving the boundary-value problem of a plane electromagnetic wave at an absorbing interface. The analyses are invariably lengthy and the resulting equations are presented in many different

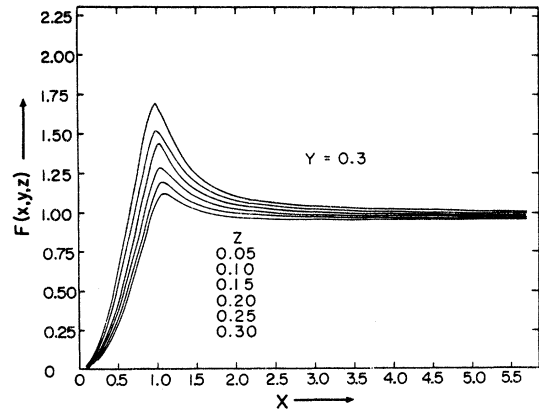


FIG. 3. Photoelectron no-loss peak intensity, relative to that for the large- ϕ region, as a function of x (which is ϕ/ϕ_c) given for a typical value of 0.3 for the absorption ratio y (which is β/δ) and illustrating the sensitivity of the maximum-intensity value to the mean free path Λ for the photoelectrons through the parameter z , which is equal to $(2\pi y \phi_c / \Lambda) \cos\theta$.

forms. An attempt is made here to summarize the results of the general solutions, specializing these for the x-ray region, and expressing the solutions in terms of a minimal set of appropriate operational parameters. Three theoretical works have been particularly helpful (along with many of their references) in reviewing the theory and in assembling the results as listed here.⁶⁻⁸

The general theory, as applied here, may be appreciably simplified because the first medium, containing the incident beam, is to be a vacuum, and because magnetic properties of the second medium have negligible effect on the x-ray interaction (permeability constant is unity). Therefore, the material constants may be completely specified by the real and imaginary components of a complex dielectric constant, viz., K' and K'' . As noted earlier, from the theory point of view, these may be derived from the quantum theory of dispersion for the x-ray region,⁵ or semiempirically by using measured photoelectric cross sections to establish values for the differential oscillator strengths which appear in the dispersion integrals.² From the experimental point of view, K' and K'' can be derived directly from reflectance curves, as will be discussed later.

In the general theory, then, factors involving the dielectric constant ϵ , the permeability constant μ , the conductivity constant σ (the notation of Ref. 7), and the frequency ν may be replaced by the real and imaginary components of a complex dielectric constant, K' and K'' , as follows⁸:

$$\epsilon\mu = K', \quad 2\mu\sigma/\nu = K'',$$

where the complex dielectric constant is given as

$$\hat{K} = K' + iK''.$$

Because throughout the x-ray region K' is only slightly less than unity, we depart from conventional notation at this point and redefine the complex dielectric constant in terms of its unit decrements, which we shall call α and γ . Henceforth,

$$\hat{K} = 1 - \alpha - i\gamma. \quad (26)$$

The formalism which we have found most convenient for the ultrasoft-x-ray region has been to express required results as functions of the grazing-incident-beam angle ϕ , of the material constants α and γ , and of a characteristic function a . Physically, this function a measures the refraction angle ϕ' for the case of the small- ϕ , $-\delta$, and $-\beta$ region, approaching a_0 , as defined in the approximate analysis given earlier. The function a is defined by

$$a^2 = \frac{1}{2} \{ \sin^2\phi - \alpha + [(\sin^2\phi - \alpha)^2 + \gamma^2]^{1/2} \}. \quad (27)$$

It can be shown that the results of the exact theories as applied to ultrasoft-x-ray reflection and

refraction (and given in Refs. 7 and 8, for example) may be expressed as follows (subscripts 1 and 2 are used, respectively, for the cases in which the incident beam is polarized with its electric vector perpendicular to the plane of incidence and parallel to the plane of incidence):

The refraction angle ϕ'_1 for energy flow (specifying the Poynting-vector direction) is given by

$$\sin\phi'_1 = a/(\cos^2\phi + a^2)^{1/2}. \quad (28)$$

The refraction angle ϕ'_2 for energy flow is given by

$$\tan\phi'_2 = \frac{2a^2(1-\alpha) + \gamma^2}{2a(1-\alpha)\cos\phi}. \quad (29)$$

(Note that the angle ϕ'_1 also specifies the direction normal to the equiphase planes in the refracting medium for both states of polarization. The equi-amplitude planes are parallel to the interface.)

The Fresnel coefficient (the ratio of reflected to incident intensity, I/I_0 , when the electric vector is perpendicular to the plane of incidence) is given by

$$R_1 = \frac{4a^2(\sin\phi - a)^2 + \gamma^2}{4a^2(\sin\phi + a)^2 + \gamma^2}. \quad (30)$$

The ratio of the Fresnel coefficients for the two states of incident-beam polarization is

$$\frac{R_2}{R_1} = \frac{4a^2(a - \cos\phi \cot\phi)^2 + \gamma^2}{4a^2(a + \cos\phi \cot\phi)^2 + \gamma^2}. \quad (31)$$

The reflection coefficient I/I_0 for an unpolarized incident beam is therefore

$$R = R_1 \left(\frac{1 + R_2/R_1}{2} \right). \quad (32)$$

In the Poynting-vector calculations for the energy flow into the refracting medium, the usual absorption factor appears, viz., $\exp[-(4\pi k/\lambda)(z/\sin\phi')]$ in which λ is the x-ray wavelength as measured in vacuum, $(z/\sin\phi')$ is the distance into the medium at the refraction angle ϕ' (of energy flow), and k is an extinction coefficient which is a function of ϕ , but is independent of the polarization state of the incident beam.

The extinction coefficient k is given by

$$k = \gamma/2(\cos^2\phi + a^2)^{1/2}. \quad (33)$$

This coefficient k becomes equal to the constant β for the small- ϕ , $-\delta$, and $-\beta$ region, as shown in the earlier analysis.

The linear x-ray absorption coefficient μ may be defined to be equal to the limiting value, as $\phi \rightarrow \frac{1}{2}\pi$, of the factor $(4\pi k/\lambda)$; therefore we have

$$\mu = \frac{4\pi}{\lambda} \frac{\gamma}{(2\{(1-\alpha) + [(1-\alpha)^2 + \gamma^2]^{1/2}\})^{1/2}}. \quad (34)$$

As mentioned earlier, with absorption involved,

the equiamplitude planes are definable as parallel to the interface. In the direction normal to these planes, i. e., the z direction, the absorption factor may be written as

$$\exp\left(-\frac{4\pi k}{\lambda \sin\phi} z\right) = \exp\left(\frac{-z}{d}\right), \quad (35)$$

where d is the depth at which the energy flow has dropped to its $(1/e)$ th value (about 37%) and is readily seen to be

$$d_1 = \lambda\alpha/2\pi\gamma \quad (36)$$

when the incident beam is polarized with its electric vector normal to the plane of incidence. In the vicinity of the "total-reflection cutoff," i. e., for $\sin\phi_c \approx \alpha^{1/2}$, this effective depth becomes

$$d_{1c} = \lambda/4\pi(\frac{1}{2}\gamma)^{1/2}. \quad (37)$$

In a nonabsorbing medium, a large illuminated volume is involved in the interference that adds up to the reflected and refracted beams. This interacting region is typically limited to a very thin layer by the effect of absorption (see below).

Finally, in order to justify the use of a complex refractive index to account for absorption in the approximate analysis (Sec. III A), let us use as a formal relationship between the complex dielectric constant and the complex refractive index,

$$n = K^{1/2}.$$

Hence, we have

$$(1 - \alpha - i\gamma) = (1 - \delta - i\beta)^2.$$

Therefore, we have

$$\alpha = 2\delta - \delta^2 + \beta^2 \quad (38)$$

and

$$\gamma = 2(1 - \delta)\beta. \quad (39)$$

When these values for α and γ thus defined in terms of δ and β are inserted into the results of the exact theory, and the small- ϕ , $-\delta$, and $-\beta$ limits are taken, the approximate results of Sec. III A follow directly.

C. Some Numerical Examples

In Fig. 4 are plotted three experimental reflection curves for the ultrasoft-x-ray region and for a gold reflector. (Gold is selected here as an example because it exhibits a relatively strong absorption effect and because evaporated samples of gold that are sufficiently continuous and without a surface oxide layer can be prepared easily.) The data for Al $K\alpha$ (8.34-Å) radiation are by Hendrick.⁹ The data for B $K\alpha$ (67.9-Å) and for Be $K\alpha$ (113.8-Å) radiations are by Lukirskii *et al.*¹⁰

The material constants α and γ for gold at these three wavelengths were obtained as those which yielded the "best fits" by the reflection function for

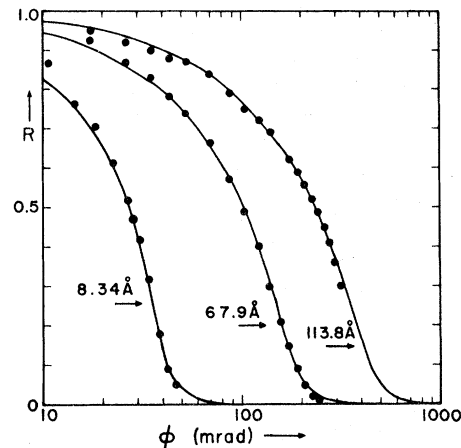


FIG. 4. Results of least-squares fitting of the exact reflection efficiency function $R(\phi)$ to the experimental data of Hendrick (Ref. 9) for Al $K\alpha$ (8.34-Å) radiation off gold and of Lukirskii *et al.* (Ref. 10) for B $K\alpha$ (67.9-Å) and Be $K\alpha$ (113.8-Å) radiations off gold. These fits yield α and γ values for gold of 13.4×10^{-4} and 4.6×10^{-4} for 8.34 Å, 2.63×10^{-2} and 1.36×10^{-2} for 67.9 Å, and 15.0×10^{-2} and 7.81×10^{-2} for 113.8 Å.

unpolarized incident radiation R [from Eq. (32)] using a standard least-squares-fitting computer program. With these constants, the required reflection-refraction parameters were then calculated by the exact functions given in Eqs. (27)–(33). These are presented in Tables I–III for wavelengths 8.34, 67.9, and 113.8 Å, respectively.

It is interesting to note that there exists an angle ϕ for which no deviation occurs in the refracted beam (i. e., the angle measured from the incident-beam direction, $\phi - \phi'$, has a zero value) and that for very small angles the refracted beam bends toward the normal. This effect is illustrated in the plots of $(\phi - \phi')$ vs ϕ presented in Fig. 5.

The effective sample depths, defined here as d_1 [Eq. (36)], have been calculated for 8.34-, 67.9-, and 113.8-Å reflections from a "thick" gold sample and are shown as a function of the incidence angle ϕ in Fig. 6. [d_1 is simply proportional to $\alpha(\phi)$, as is given in Tables I–III.]

As a test of the use of such an effective-depth measure d_{1c} , and to illustrate the additional effect of a thin-film interference, the reflection curve has been calculated² (and is plotted in Fig. 7) for 8.34-Å reflection from aluminum with varying thickness of Al_2O_3 (oxide film) on the surface. (This reflection model is idealized in that it is assumed that there is a sharp "break" in density and chemistry between the oxide film and the aluminum substrate.) The value of γ used to characterize the Al_2O_3 material yielded an effective-depth estimate

TABLE I. Al $K\alpha$ (8.34-Å) x-ray reflection-refraction characteristics for a gold surface using α and γ values of 13.4×10^{-4} and 4.6×10^{-4} , respectively, determined by fitting $R(\phi)$ to experimental reflection data as shown in Fig. 4. Given here are the characteristic function a as calculated from Eq. (27); the reflection efficiencies for the two states of polarization and for an unpolarized incident beam, R_1 , R_2 , and R , respectively, as calculated from Eqs. (30)–(32); the deviation of the refracted-beam from the incident-beam direction for the energy flow within the medium, $\phi - \phi'$, for the two states of polarization, as calculated from Eqs. (28) and (29); and the extinction coefficient k as calculated from Eq. (33). Presented in the last three columns are the percent errors which are made by using the approximate rather than the exact theory by replacing $\sin\phi'_1$ by a_0 [Eq. (13)], by replacing R by R_0 [from Eq. (19)], and by replacing k by β [from Eqs. (38) and (39)]. [Note: Usually the largest errors are made in the determination of the optical constants from reflectance data by using the approximate rather than the exact expression $R(\phi)$ (see Sec. III).]

ϕ (mrad)	a	R	$R_1 - R_2$		$\phi - \phi'_1$ (mrad)	$\phi - \phi'_2$ (mrad)	$10^4 k$	$a_0 - \sin\phi'_1$		$R_0 - R$		$\beta - k$	
			R_1 (%)	R_2 (%)				a_0 (%)	R (%)	k (%)	β (%)		
0	0.006	1.000	0.000	0.000	-6.192	-6.209	2.298	0.053	0.000	0.000	0.069	0.069	0.069
10	0.006	0.834	0.026	0.026	3.578	3.561	2.299	0.047	0.010	0.010	0.064	0.064	0.064
20	0.007	0.664	0.058	0.058	12.704	12.690	2.299	0.030	0.021	0.021	0.050	0.050	0.050
30	0.010	0.442	0.119	0.119	20.087	20.076	2.299	0.007	0.038	0.038	0.027	0.027	0.027
40	0.020	0.145	0.317	0.317	20.144	20.139	2.300	...	0.079	0.079	0.007	0.007	0.007
50	0.035	0.038	0.693	0.693	15.297	15.294	2.300	0.005	0.202	0.202	0.002	0.002	0.002
60	0.048	0.015	1.143	1.143	12.209	12.207	2.300	0.020	0.356	0.356	0.001	0.001	0.001
70	0.060	0.007	1.665	1.665	10.199	10.197	2.300	0.040	0.533	0.533	0.001	0.001	0.001
80	0.071	0.004	2.262	2.262	8.778	8.777	2.300	0.064	0.736	0.736	0.001	0.001	0.001
90	0.082	0.002	2.933	2.933	7.716	7.715	2.300	0.092	0.964	0.964
100	0.093	0.001	3.679	3.679	6.888	6.887	2.300	0.123	1.219	1.219
200	0.195	...	14.926	14.926	3.332	3.331	2.300	0.621	5.240	5.240
300	0.293	...	31.679	31.679	2.174	2.174	2.300	1.450	11.905	11.905
400	0.388	...	51.301	51.301	1.588	1.588	2.300	2.603	20.848	20.848
500	0.478	...	70.696	70.696	1.228	1.228	2.300	4.073	30.770	30.770

d_{1c} by Eq. (37) of 150 Å in the angular region of "total-reflection" cutoff.

As noted earlier and indicated in the conventional x-ray reflection-refraction theory presented as

an approximate solution in Sec. IIIA, $\sin\phi'_1$ is approximated as a_0 [Eq. (13)]; the reflection coefficient R for unpolarized incident radiation is approximated as R_0 [Eq. (19)]; and the extinction co-

TABLE II. B $K\alpha$ (67.9-Å) x-ray reflection-refraction characteristics for a gold surface using α and γ of 2.63×10^{-2} and 1.36×10^{-2} respectively, and as determined by fitting $R(\phi)$ to experimental reflection data as shown in Fig. 4. Characteristic values were then calculated as described for Table I.

ϕ (mrad)	a	R	$R_1 - R_2$		$\phi - \phi'_1$ (mrad)	$\phi - \phi'_2$ (mrad)	$10^4 k$	$a_0 - \sin\phi'_1$		$R_0 - R$		$\beta - k$	
			R_1 (%)	R_2 (%)				a_0 (%)	R (%)	k (%)	β (%)		
0	0.041	1.000	0.000	0.000	-40.662	-42.991	67.934	1.117	0.000	0.000	1.421	1.421	1.421
20	0.041	0.894	0.327	0.327	-20.947	-23.261	67.947	1.094	0.122	0.122	1.402	1.402	1.402
40	0.042	0.795	0.668	0.668	-1.836	-4.103	67.985	1.025	0.247	0.247	1.345	1.345	1.345
60	0.043	0.701	1.039	1.039	16.564	14.376	68.049	0.913	0.382	0.382	1.251	1.251	1.251
80	0.046	0.608	1.464	1.464	34.035	31.962	68.137	0.761	0.532	0.532	1.120	1.120	1.120
100	0.050	0.513	1.981	1.981	50.165	48.247	68.247	0.576	0.705	0.705	0.957	0.957	0.957
120	0.055	0.413	2.659	2.659	64.179	62.461	68.376	0.376	0.914	0.914	0.766	0.766	0.766
140	0.065	0.309	3.622	3.622	74.634	73.161	68.516	0.193	1.177	1.177	0.561	0.561	0.561
160	0.080	0.205	5.083	5.083	79.342	78.145	68.646	0.077	1.538	1.538	0.370	0.370	0.370
180	0.101	0.122	7.225	7.225	77.324	76.382	68.743	0.045	2.110	2.110	0.228	0.228	0.228
200	0.127	0.070	9.958	9.958	71.359	70.607	68.800	0.070	2.975	2.975	0.145	0.145	0.145
220	0.153	0.042	13.068	13.068	64.738	64.117	68.832	0.139	4.065	4.065	0.099	0.099	0.099
240	0.178	0.026	16.431	16.431	58.747	58.216	68.850	0.244	5.304	5.304	0.072	0.072	0.072
260	0.202	0.018	19.990	19.990	53.593	53.128	68.862	0.378	6.662	6.662	0.056	0.056	0.056
280	0.226	0.012	23.714	23.714	49.192	48.778	68.870	0.535	8.125	8.125	0.044	0.044	0.044
300	0.249	0.009	27.579	27.579	45.414	45.039	68.875	0.711	9.689	9.689	0.036	0.036	0.036
400	0.355	0.002	48.153	48.153	32.499	32.246	68.889	1.834	18.808	18.808	0.016	0.016	0.016
500	0.451	0.001	68.497	68.497	24.884	24.695	68.894	3.307	29.069	29.069	0.009	0.009	0.009
600	0.541	...	85.497	85.497	19.755	19.606	68.896	5.102	37.509	37.509	0.006	0.006	0.006
700	0.624	...	96.546	96.546	15.990	15.870	68.897	7.203	39.167	39.167	0.004	0.004	0.004

TABLE III. Be $K\alpha$ (113.8-Å) x-ray reflection-refraction characteristics for a gold surface using α and γ of 15.0×10^{-2} and 7.81×10^{-2} , respectively, as determined by fitting $R(\phi)$ to experimental reflection data shown in Fig. 4. Characteristic values were then calculated as described for Table I.

ϕ (mrad)	a	R	$R_1 - R_2$	$\phi - \phi'_1$ (mrad)	$\phi - \phi'_2$ (mrad)	$10^4 k$	$a_0 - \sin \phi'_1$	$R_0 - R$	$\beta - k$
			R_1 (%)				a_0 (%)	R (%)	k (%)
0	0.098	1.000	0.000	-97.474	-133.656	388.576	6.586	0.000	8.859
40	0.098	0.904	1.561	-58.013	-94.049	388.866	6.500	0.555	8.778
80	0.100	0.815	3.153	-19.670	-55.262	389.738	6.240	1.126	8.535
120	0.102	0.731	4.833	17.431	-17.405	391.190	5.811	1.730	8.132
160	0.106	0.650	6.672	53.056	19.307	393.221	5.218	2.391	7.573
200	0.111	0.570	8.763	86.807	54.514	395.821	4.473	3.136	6.867
240	0.119	0.489	11.237	118.034	87.608	398.964	3.602	4.000	6.025
280	0.130	0.407	14.297	145.666	117.567	402.590	2.653	5.031	5.070
320	0.145	0.322	18.250	167.962	142.686	406.564	1.719	6.288	4.043
360	0.168	0.239	23.536	182.362	160.360	410.606	0.946	7.859	3.018
400	0.200	0.163	30.583	186.318	167.790	414.250	0.482	9.935	2.112
440	0.241	0.104	39.334	180.074	164.753	417.036	0.340	12.850	1.430
480	0.286	0.064	49.038	167.769	155.033	418.889	0.439	16.710	0.982
520	0.333	0.041	58.819	153.757	142.980	420.059	0.735	21.168	0.700
560	0.378	0.027	68.087	140.255	130.958	420.814	1.194	25.744	0.519
600	0.421	0.018	76.493	127.960	119.814	421.323	1.787	29.985	0.398
700	0.520	0.008	92.379	102.575	96.442	422.050	3.705	36.169	0.225
800	0.607	0.005	99.459	83.018	78.223	422.419	6.094	31.102	0.137
900	0.683	0.003	97.161	67.305	63.499	422.634	8.855	13.507	0.087
1000	0.749	0.003	86.346	54.155	51.134	422.770	11.938	10.509	0.054

efficient k is approximated as β . In the last three columns of Tables I-III, the percentage errors that are made by these approximations are presented for the 8.34-, 67.9-, and 113.8-Å x-ray interactions.

IV. APPLICATION TO DETERMINATION OF MATERIAL CONSTANTS α , γ , AND Λ

A. Reflection-Intensity Measurements

The approximate theory, as given in Sec. III A, including the reflection equation R_0 , has been used exclusively in the x-ray region for the determination of optical constants from reflectance data (see Refs. 9 and 10 for examples). As has been illustrated in Tables I-III, the approximate theory is satisfactory for x-ray wavelengths less than 10 Å. However, it is also indicated that for wavelengths greater than 50 Å, significantly large errors may well result from this practice. In fact, in this long-wavelength region, we have found that errors as great as 45% have been made by not using the more exact theory in the determination of the linear absorption coefficient from reflection measurements.

The results of an application of the exact theory as presented in Sec. III B above to the determination of optical constants for the ultrasoft-x-ray region from reflection measurements are presented in Table IV. Here the constants α and γ were determined by least-squares fitting of the reflection

function R [Eq. (32)] to the reflectance data of Lukirskii *et al.*¹⁰ for the B $K\alpha$ (67.9-Å) x radiation from lithium fluoride, magnesium fluoride, and evaporated films of carbon, aluminum, silver, and gold. With these constants, the linear absorption coefficients were calculated, using Eq. (34). By assuming sample density values as indicated, the mass absorption coefficients were calculated. These (μ/ρ) values were compared to those derived from transmission measurements.^{10,11} Also presented in Table IV are the effective-depth estimates d_{1c} , for each of these samples.

B. Photoelectron-Intensity Measurements

As a test of the refraction theory discussed above and of the model described in Sec. II for photoelectron production, and to illustrate a new method for measuring electron mean free paths, we have compared the theoretical with the experimental photoelectron-intensity-vs- ϕ results.

In our electron spectrograph (described previously^{4,12}) a thick evaporated gold sample was irradiated by an 8.34-Å x-ray beam which departed from being a parallel beam by about ± 4 mrad. The intensity of the Au $4f_{7/2}$ (1404-eV) photoelectron line was measured as a function of the angle ϕ , as was illustrated in Fig. 2. As established above and presented in Table I, the approximate theory of Sec. III A can be appropriately applied to an interpretation of this 8.34-Å grazing-incidence interaction at a gold interface. From fitting the reflection

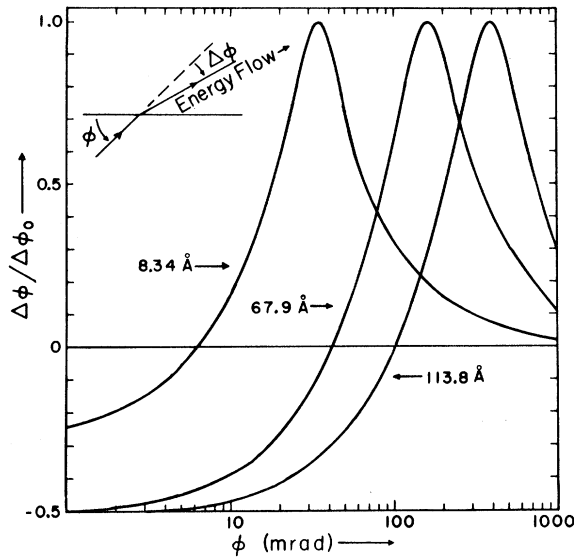


FIG. 5. Plots of the deviation of the refracted beam within gold from the incident-beam direction for the three wavelengths 8.34, 67.9, and 113.8 Å. The deviation angle $\phi - \phi'$ (defined here as $\Delta\phi$) was calculated from Eq. (28) for the direction of energy flow (that of the Poynting vector) for the refracted beam resulting from the incident-beam component which is polarized with its electric vector normal to the plane of incidence. $\Delta\phi$ is plotted here as relative to its maximum value, near ϕ_c , or $\Delta\phi_0$, given by 20.2, 80, and 186 mrad, respectively, for the 8.34-, 67.9-, and 113.8-Å wavelengths. (It is interesting to note here that the refracted beam bends toward the normal for the smaller angles of incidence.)

data as presented in Fig. 4, values for α and γ were determined which yielded the values for δ , β , and β/δ as 6.7×10^{-4} , 2.3×10^{-4} , and 0.29, respectively.

The ratio of the "no-loss" photoelectron line intensity to its constant value for the large- ϕ region, viz., $F(x, y, z)$, was plotted as a family of curves [using Eq. (21)] for this example with a β/δ value (i. e., γ) of 0.3, and was presented in Fig. 3. These curves demonstrate that the maximum in the photoelectron line intensity near the critical angle ϕ_c has a value which is relatively sensitive to the parameter z —also sensitive, therefore, to the electron mean-free-path value Λ [see Eq. (24)]. In fact, Λ may be measured simply as a function of F_m , the ratio of the experimental intensity at its maximum value to its value which is constant at large angle ϕ . Because this maximum is not sharp, this ratio can be measured accurately even with a relatively divergent x-ray beam.

The experimental value of this ratio, F_m , was 1.39. By matching at the maximum in the intensity near critical angle ϕ_c in our curve fitting, with Eq. (20) or Eq. (21), we obtain a value of 5.2

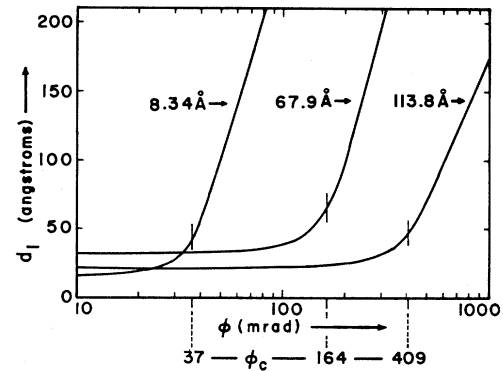


FIG. 6. Effective-depth values d_1 at which the energy flow normal to the surface (and to the equiamplitude planes) has dropped to its $(1/e)$ th value within gold and for the three wavelengths 8.34, 67.9, and 113.8 Å. These were calculated, using Eq. (36), for the incident-beam component that is polarized with its electric vector normal to the plane of incidence. d_1 is simply proportional to the function $\alpha(\phi)$, as given in Tables I–III. The angular region for reflection "cutoff" for each wavelength is indicated here by the corresponding ϕ_c values.

$\times 10^{-3}$ for $\mu(\cos\theta)/\epsilon$, or, equivalently, a value of 0.14 for the parameter z . The resulting curve fit is shown in Fig. 8.

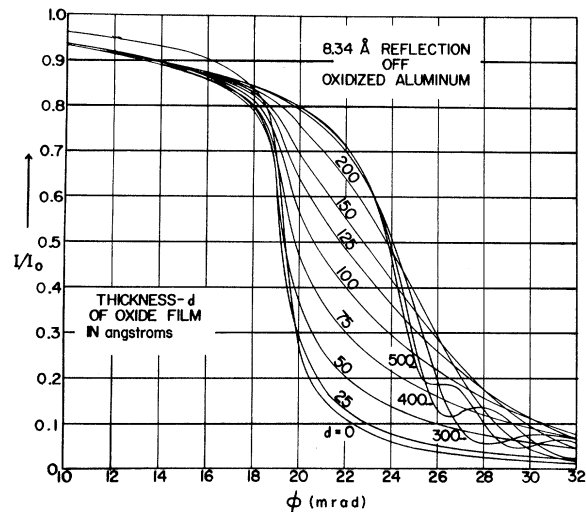


FIG. 7. Illustrating the effect upon the reflection of 8.34-Å radiation of the thin-film depth of aluminum oxide upon an aluminum substrate. These curves were calculated, using the approximate theory as presented in Sec. III A, as applied to a three-media model. The δ , β , and mass density ρ values assumed for Al_2O_3 were, respectively, 28.5×10^{-5} , 2.10×10^{-5} , and 3.50 g/cm^3 . The corresponding values for Al were, respectively, 18.1×10^{-5} , 0.57×10^{-5} , and 2.70 g/cm^3 .

TABLE IV. Comparison of the mass absorption coefficients for B K α (67.9- \AA) x rays as calculated from reflectance data and as determined directly by transmission measurements. α and γ values were determined by fitting $R(\phi)$ to the reflection data of Lukirskii *et al.* (Ref. 10). The linear absorption coefficients were calculated from Eq. (34) and the μ/ρ values were derived using assumed surface-density values as listed. As calculated from Eq. (37) effective-depth estimates are presented for the grazing-incidence angle ϕ_c around "cutoff" (ϕ_c is defined from the relation $\sin\phi_c = \alpha^{1/2}$).

Reflection sample	Assumed density (g/cm ³)	10 ³ α	10 ³ γ	(μ/ρ) _{Reflection} (10 ⁻⁴ cm ² /g)	(μ/ρ) _{Transmission} (10 ⁻⁴ cm ² /g)	Transmission measurement references	Effective sample depth d_{1c} (\AA)
C	2.0	13.0	1.27	0.60	0.62	Henke <i>et al.</i> (Ref. 11)	210
Al	2.7	19.2	13.8	4.83	6.59 6.89	Henke Lukirskii <i>et al.</i> (Ref. 10)	65
Ag	10.5	32.0	9.01	0.82	0.64	Lukirskii	80
Au	19.3	26.3	13.6	0.67	0.67	Lukirskii	65
LiF	2.64	16.2	5.83	2.12	2.61	Henke	100
MgF ₂	3.15	10.5	12.7	3.73	3.76	Henke	68

We may use these results to determine a value for the mean free path of 1.4-keV electrons in gold by solving for Λ in the relation presented in (24) above, yielding

$$\Lambda = z\lambda/2\pi y\phi_c \cos\theta. \quad (40)$$

Substituting in (40) the appropriate values for z , λ , y , ϕ_c , and θ as 0.14, 8.34 \AA , 0.29, 0.037 rads, and 21 $^\circ$, respectively, we obtain 19 \AA for the mean free path Λ . This value is in relatively good agreement with a recent measurement for the mean

free path in gold of 22 ± 4 \AA by an Uppsala group¹³ using direct transmission and emission measurements on calibrated evaporated gold films with 1.2-keV electrons.

V. CONCLUSION

Because magnetic effects are negligible in the x-ray region, one may apply directly a general theory for the reflection and refraction of a plane electromagnetic wave at an absorbing dielectric interface. Although their derivations are typically long and tedious, the results of this theory can be written for application in the x-ray region in relatively simple form, as summarized here in Eqs. (27)–(37), in terms of the grazing-incidence angle ϕ , two material constants α and γ , and the function $a(\phi)$ which becomes the angle of refraction ϕ' for the small- ϕ region. The optical constants α and γ can be identified as the unit decrements to a complex dielectric constant defined as

$$\hat{K} = 1 - \alpha - i\gamma.$$

These constants can be determined theoretically from the quantum-mechanical dispersion theory as developed for the x-ray region, or experimentally by fitting x-ray reflectance data.

When these results are approximated for the small- ϕ , $-\alpha$, and $-\gamma$ values, the conventional equations for x-ray reflection and refraction are obtained as those derived above in Sec. III A, using the traditional complex dielectric-constant method. It may be noted that in this region (generally applicable for wavelengths less than 10 \AA) the reflection-efficiency-vs- ϕ characteristic is the same for both states of polarization of the incident

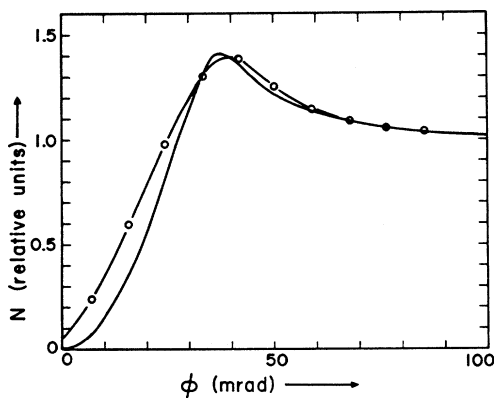


FIG. 8. Fitting of the experimental no-loss photoelectron-intensity-vs- ϕ curve with that predicted theoretically by Eq. (20) in order to determine a mean-free-path value for 1.4-keV electrons within gold. The x-ray-beam divergence was ± 4 mrad, which effect was made small by matching the curves in the "flat" regions, viz., at the maximum near ϕ_c and in the constant large- ϕ region. These data yielded a mean-free-path value Λ of 19 \AA .

beam, i. e., for its electric vector perpendicular and parallel to the plane of incidence; also, the direction of the Poynting vector (energy-flow direction) within the medium is the same for both states of polarization and is normal to the equiphase planes. A linear x-ray absorption coefficient may be defined as $4\pi\beta/\lambda$, which is independent of the grazing-incidence angle ϕ .

For wavelengths greater than about 50 \AA , measurable deviations from the predictions of this approximate theory become evident. The reflection-efficiency-vs- ϕ characteristic is significantly different for each state of polarization for the incident beam. Also, the angle of refraction ϕ' is different for each of these incident-beam polarized components, with only one direction being normal to the equiphase planes (that which corresponds to the incident beam with its electric vector perpendicular to the plane of incidence). Finally, the extinction coefficient k and, equivalently, the linear x-ray absorption coefficient μ are definable only as functions of the angle ϕ in this long-wavelength region. The question of when such effects as these need to be taken into account in a given ultrasoft-x-ray measurement can be resolved by applying the equations which have been summarized here.

The exact Fresnel equations for reflection do yield satisfactory fits to the experimental data for the ultrasoft-x-ray region and can be used to establish the optical constants α and γ . Similarly, the linear absorption coefficients for normal incidence can be deduced from reflectance data. Examples of such x-ray absorption coefficients, as determined from reflection measurements, have been shown to be in reasonably good agreement with those determined from direct transmission measurements.

In this work, in order to test the refraction theory, the theoretical prediction of the yield of "no-loss" photoelectrons as excited by the refracted

beam has been shown to be in reasonably good quantitative agreement with electron spectrographic measurements. In this case, the fitting of the theoretical and the experimental curves yields the electron mean-free-path value Λ . One comparison has been possible of a mean-free-path value as deduced using the model given here for the production of no-loss photoelectrons by the refracted beam with a mean-free-path value as obtained from direct transmission and emission measurements. The agreement was reasonably good.

New and important techniques based upon low-energy x-ray and electron spectroscopy^{14,15} are now being considered by many laboratories for the physical and chemical characterization of surfaces. For these new methods to be quantitative, cross-section data for both x-ray and electron absorption must be available. Only in recent years has there been a significant amount of ultrasoft-x-ray absorption data reported. Electron-absorption data for solids, and for this 100–1000-eV region (such as ionization cross sections or mean-free-path values), are essentially nonexistent at this time. The determination of these cross sections by transmission measurements is very difficult because of the requirement for very thin samples. For this reason, the methods which have been described here for the determination of μ and Λ by ultrasoft-x-ray reflection, refraction, and photoelectron excitation may be of considerable practical value.

ACKNOWLEDGMENTS

The author is pleased to acknowledge the invaluable assistance in this work of Andrew Hwang, Lois McAllister, Therese McElhaney, and R. Srinivasan. He is indebted to Dr. M. R. Lefèvre, of Université des Sciences de Lille, for a very helpful conversation concerning her recent work with Professor Marc Montel on the general theory of the reflection and refraction of electromagnetic radiation.

*Work supported by U. S. Air Force Office of Scientific Research Grant No. AFOSR 72-1274.

¹L. G. Parratt, *Phys. Rev.* **95**, 359 (1954).

²B. L. Henke and J. C. Miller, U. S. Air Force Office of Scientific Research Report No. TN-59-895, 1959 (unpublished).

³B. L. Henke and J. W. M. DuMond, *J. Appl. Phys.* **26**, 903 (1955).

⁴B. L. Henke and M. W. Anderson, in *Proceedings of the Sixth International Conference on X-Ray Optics and Microanalysis*, Osaka, Japan, 1971 (unpublished).

⁵A. H. Compton and S. K. Allison, *X-Rays in Theory and Experiment*, 2nd ed. (Van Nostrand, New York, 1935), p. 305.

⁶A. I. Mahan, *J. Opt. Soc. Am.* **46**, 913 (1956).

⁷M. R. Lefèvre, *Opt. Acta* (to be published).

⁸W. R. Smythe, *Static and Dynamic Electricity*, 3rd

ed. (McGraw-Hill, New York, 1968).

⁹R. W. Hendrick, *J. Opt. Soc. Am.* **47**, 165 (1957).

¹⁰A. P. Lukirskii *et al.*, *Opt. Spectry. (USSR)* **16**, 168 (1964).

¹¹B. L. Henke and R. L. Elgin, *Advances in X-Ray Analysis*, edited by B. L. Henke, J. B. Newkirk, and G. R. Mallett (Plenum, New York, 1970), Vol. 13, p. 639.

¹²B. L. Henke and R. E. Lent, in Ref. 11, Vol. 12, p. 480.

¹³Y. Baer *et al.*, *Solid State Commun.* **8**, 1479 (1970).

¹⁴B. L. Henke, in Ref. 11, Vol. 13, p. 1.

¹⁵K. Siegbahn *et al.*, *ESCA, Atomic, Molecular and Solid State Structure Studied by Means of Electron Spectroscopy* (Almqvist & Wiksells boktryckeri AB, Uppsala, Sweden, 1967).